Exact and adiabatic solutions for a spinless Peierls-Hubbard model in a finite cluster

Miguel Cardenas, David Gottlieb, and Jaime Rössler
Departamento de Física, Facultad de Ciencias, Universidad de Chile, Casilla 653, Santiago, Chile
(Received 5 May 1993)

The exact solution of the Hubbard-Peierls model is given in a cluster of six atoms and three spinless electrons. Phonons with wave vector $k=\pi$ are retained and quantum mechanically analyzed. Energy level and several averages are evaluated, thus determining the physical properties of the model in terms of the parameters of the system. The regime of the distorted lattice is obtained. The exact and Born-Oppenheimer (BO) results are compared, concluding that the BO *enhances* quantum fluctuations; this peculiar behavior is explained.

I. INTRODUCTION

It is well known that one-dimensional metals may spontaneously break translational symmetry. In fact, electron-electron (*e-e*) or electron-phonon (*e*-ph) interactions may give rise to spin, charge, or bond waves at low temperatures, producing an insulating phase. In particular, the low-symmetry phase is called the "Peierls distortion" when the role of *e*-ph interaction is essential. On the other hand, quantum fluctuations are especially important in a one-dimensional topology, thus implying the absence of long-range order (with the possible exception of zero-temperature case). Therefore, a mean-field treatment (like the adiabatic approximation for latter displacements) is not reliable in one dimension.[1] Nevertheless, many papers have analyzed the Peierls distortion by considering the lattice displacements as classical variables,[2-10] whereas relatively few authors have considered the lattice degrees of freedom as true quantum operators.[11-16]

The validity of adiabatic approximation rests on the relatively long lattice vibration time, as compared with the electronic transference time. However, the latter can be considerably increased due to *e-e* interactions. In particular, in the case of a strong intramolecular Coulomb repulsion (equivalent to a system of spinless electrons[17]), the Peierls distortion can disappear due to the effect of quantum fluctuations.[11] In what follows, we shall briefly summarize some known results for the Peierls distortion.

A. Adiabatic results

An infinite one-dimensional system with nearest-neighbor electronic transference is always distorted in the absence of *e-e* interactions,[18] no matter how small the *e*-ph coupling is.[2,3]

In the case of a half-filled band, the effect of intramolecular Coulomb repulsion, U, is to enhance Peierls distortions if $U<\{\text{Bandwidth}\}$; while a further increase in U inhibits the bond wave (BW) state [4,6]. For an arbitrary band filling and small U, the wave vector of the Peierls distortion corresponds to $2k_F$, while a large U leads to a $4k_F$ distortion.[19]

We now consider the effect of a nearest-neighbor Coulomb interaction, G. For a half-filled band, in the case $G<\frac{1}{2}U$, the BW is enhanced by G, while, for $G>\frac{1}{2}U$, an intramolecular charge wave (CW) is stabilized.[6,8] The effect of second-neighbor Coulomb repulsion is opposite to G. For the case of $[CH]_n$, it has been claimed that the Peierls distortion proceeds mainly from the *e-e* interaction, while the *e*-ph coupling plays a minor role.[20]

In the case of a $\frac{1}{4}$-filled electronic band and $U\rightarrow\infty$ (or equivalently, a half-filled band of spinless electrons), a small G enhances the BW state compared with the $G=0$ case, while a larger G tends to inhibit BW. For $G>2t$ a CW may appear if G prevails over *e*-ph interaction; also, coexistence between a CW and a BW becomes possible.[9,10] For a finite (but large) repulsion U, a period-4 spin wave appears superposed on the period-2 BW; the spins rest on the bonds.[5]

B. The effect of phononic quantum fluctuations

Most knowledge of nonadiabatic behavior is due to Monte Carlo simulations[11-14] for moderately large clusters and low temperature. A few studies use exact diagonalization of small (two sites) clusters.[15,16] All of these works consider a half-filled band, which leads to a period-2 BW (dimerized lattice).

A system of (spin-$\frac{1}{2}$) noninteracting electrons is *always dimerized,* including the case of an infinitesimal *e*-ph coupling.[11,12] This behavior holds for two different cases: the molecular crystal and the Su-Schrieffer-Heeger (SSH) (Ref. 2) models. In the first case, electrons are coupled to intramolecular vibrations, while in the SSH model the *e*-ph coupling is due to the variations in the intermolecular distances, which change the electronic transfer energy.

A system of noninteracting spinless fermions is dimerized only if the *e*-ph coupling S surpasses a critical value,[11,12] say $S>S_c$. Obviously S_c increases with the phonon frequency.

When the intramolecular repulsion U is introduced in the SSH model, and the phonon frequency is small, a first increase in U enhances the BW, while a further increase

inhibits it. For larger phonon frequencies, an increase in U *always* reduces the dimerization.[13] The effect of nearest-neighbor repulsion has seldom been studied in the nonadiabatic case; however, calculations for $G=U/2$ show a strong enhancement of the BW over the $G=0$ case.[13]

For the molecular crystal model and spin-$\frac{1}{2}$ electrons, the effect of U is *always* to decrease distortion, which disappears up to a critical value $U>U_c$. The effect of G is opposite to U, strongly enhancing the Peierls phase.[13]

In the present work we analyze the exact (nonadiabatic) solution of the SSH model (intersite e-ph coupling) in a six-site ring. Also, the first-neighbor e-e repulsion G is included. The case of three spinless fermions is considered (which is equivalent to a $\frac{1}{4}$-filled band of spin-$\frac{1}{2}$ electrons in the $U=\infty$ limit[17]). Therefore, the lattice may be unstable under a period-2 BW. Accordingly, we only retain phonons with wave vector $k=\pi$.

Our aim is to determine and characterize the distorted and undistorted regions in the parameter space. Finite-size effects tend to reduce the BW region for our six-site ring.[7] Despite this shortcoming, the exact quantum-mechanical results provide some advantages in relation to Monte Carlo simulations, as we can obtain the energy spectrum which allows us to evaluate the softening in phononic frequency, and the quantum fluctuation time of a BW. In addition, our approach demands insignificant CPU time.

Our work is organized as follows: In Sec. II the model is described, and its solution is formally presented using group theory. In Sec. III we analyze the adiabatic limit, where the Born-Oppenheimer (BO) approximation is suitable. In Sec. IV the numerical results are presented; the exact quantum-mechanical calculations are compared with the BO approximation. Finally, Sec. V summarizes the conclusions of the work.

II. THE MODEL

We consider the generalized Hubbard-SSH model for the spinless electrons in a six-site ring. The Hamiltonian is

$$H=-\sum_{l}^{N}[t-(-1)^{l}u](c_l^{\dagger}c_{l-1}+c_{l-1}^{\dagger}c_l) +G\sum_{l}n_{l-1}n_l+\omega(b^{\dagger}b+\tfrac{1}{2}) . \quad (1)$$

here $c_l^{\dagger}$ creates an electron at site l; $n_l=c_l^{\dagger}c_l$ is the associated number operator; $N=6$; t and G are the first-neighbor electronic hopping amplitude and Coulomb repulsion, respectively; $b^{\dagger}$ is the creation operator for a phonon with momentum $k=\pi$; and $u=S(b+b^{\dagger})/\sqrt{N}$ is the lattice displacement. Finally, ω and S are the phonon frequency and e-ph coupling, respectively. We shall use $t=1$ as energy scale.

The e-ph coupling proceeds from the fact that the electronic transfer energy $t_{l-1,l}$ decreases as intersite distance q_l-q_{l-1} increases. In Eq. (1) the linear approximation is considered: $t_{l-1,l}=t-\alpha(q_l-q_{l-1})\equiv t-(-1)^{l}u$. This approximation, however, breaks down for large lattice deformations $(-1)^{l}u>t$, since a further increase in intersite distance leads to an *increase* in $|t_{l-1,l}|$. In that case our model loses physical meaning.[21]

Our cluster of six atoms and three electrons has 20 electronic states. We separate these states in terms of the irreducible representations (IR's) of the associated symmetry group, C_{6v}, concluding that the electronic Hilbert space splits into six subspaces of IR's; in Tinkham's notation,[22] they are

$$\mathcal{H}=A_1\oplus 3A_2\oplus 3B_1\oplus B_2\oplus 3E_1\oplus 3E_2 .$$

As an example, the basis for the IR's B_2 and A_2 are

$$|B_2\rangle=\sqrt{\tfrac{1}{12}}[c_1^{\dagger}(c_2^{\dagger}+c_6^{\dagger})c_4^{\dagger}-c_2^{\dagger}(c_3^{\dagger}+c_1^{\dagger})c_5^{\dagger}\pm\text{cyclic}]|0\rangle , \quad (2)$$

$$\begin{aligned}|A_2,1\rangle&=\sqrt{\tfrac{1}{2}}[c_1^{\dagger}c_3^{\dagger}c_5^{\dagger}+c_2^{\dagger}c_4^{\dagger}c_6^{\dagger}]|0\rangle ,\\ |A_2,2\rangle&=\sqrt{\tfrac{1}{6}}[c_1^{\dagger}c_2^{\dagger}(c_6^{\dagger}+c_3^{\dagger})+c_3^{\dagger}c_4^{\dagger}(c_2^{\dagger}+c_5^{\dagger})\\ &\quad+c_5^{\dagger}c_6^{\dagger}(c_4^{\dagger}+c_1^{\dagger})]|0\rangle ,\\ |A_2,3\rangle&=\sqrt{\tfrac{1}{12}}[c_1^{\dagger}(c_2^{\dagger}-c_6^{\dagger})c_4^{\dagger}+c_2^{\dagger}(c_3^{\dagger}-c_1^{\dagger})c_5^{\dagger}\\ &\quad+\text{cyclic}]|0\rangle ,\end{aligned} \quad (3)$$

where $|0\rangle$ is the vacuum state. By means of transformation $c_l^{\dagger}\rightarrow(-1)^{l}c_l^{\dagger}$, the basis of IR A_2 goes over IR B_1, and also $B_2\rightarrow A_1$, $E_1\rightarrow E_2$.

The phonon operators b and $b^{\dagger}$ belong to the B_1 IR. Thus the e-ph coupling mixes the electronic subspaces of IR's in pairs, giving rise to three true invariant subspaces:

$$\mathcal{H}_1=A_1\oplus 3B_1 , \quad \mathcal{H}_2=3A_2\oplus B_2 , \quad \mathcal{H}_3=3E_1\oplus 3E_2 . \quad (4)$$

The eigenstates of H belonging to $\mathcal{H}_2$ can be expressed in terms of the basis displayed in Eqs. (2) and (3), $\Psi_E=\sum_n[\beta_n|B_2\rangle+\sum_{j=1}^{3}\gamma_{j,n}|A_2,j\rangle]|n\rangle$ where $|n\rangle=(b^{\dagger})^n|0\rangle/\sqrt{n!}$ and E is the eigenvalue. In spite of the superposition between two IR's of C_{6v} appearing in Eq. (4), a given eigenstate of H classified by *only one* IR of C_{6v}, but now the symmetry operations of this group involve both electronic and phononic degrees of freedom. For example, in the case of $\mathcal{H}_2$, the IR of Ψ_E may be B_2 or A_2. In the first case $\beta_{2n+1}=0=\gamma_{j,2n}$, while for the IR A_2 it holds that $\beta_{2n}=0=\gamma_{j,2n+1}$.

There are two important limiting cases in our model.

(i) The limit $G\rightarrow\infty$, where the associated states are "charge waves" (CW's). One of them is $|\text{CW},1\rangle=c_1^{\dagger}c_3^{\dagger}c_5^{\dagger}|0\rangle$; that is, electrons are in the odd sites, while even sites are empty. The other CW state is $|\text{CW},2\rangle=c_2^{\dagger}c_4^{\dagger}c_6^{\dagger}|0\rangle$.

In the limiting case when lattice distortion cuts off half of the electronic transferences, say $t=|u|$, the ground state (GS) is a full dimerized BW. When $t_{2l,2l+1}=0$, the GS is $|\text{BW},1\rangle\equiv b_1^{\dagger}b_3^{\dagger}b_5^{\dagger}|0\rangle$, while for $t_{2l-1,2l}=0$ the GS is $|\text{BW},2\rangle\equiv b_2^{\dagger}b_4^{\dagger}b_6^{\dagger}|0\rangle$. Here state $b_l=(c_l+c_{l+1})/\sqrt{2}$ links sites l and $l+1$. States $|\text{BW},1\rangle$ and $|\text{BW},2\rangle$ are not orthogonal to each other.

We project the CW and BW states over the IR's of C_{6v}, obtaining

$$
\begin{aligned}
&|\mathrm{CW},+\rangle \equiv [|\mathrm{CW},2\rangle + |\mathrm{CW},1\rangle]/\sqrt{2} = |A_2,1\rangle \ , \\
&|\mathrm{CW},-\rangle \equiv [|\mathrm{CW},2\rangle - |\mathrm{CW},1\rangle]/\sqrt{2} = |B_1\rangle \ , \\
&|\mathrm{BW},+\rangle \equiv \sqrt{\tfrac{2}{5}}[|\mathrm{BW},2\rangle + |\mathrm{BW},1\rangle] \\
&\qquad = \sqrt{\tfrac{2}{5}}|A_2,1\rangle + \sqrt{\tfrac{3}{5}}|A_2,3\rangle \ , \\
&|\mathrm{BW},-\rangle \equiv \sqrt{\tfrac{2}{3}}[|\mathrm{BW},2\rangle - |\mathrm{BW},1\rangle] = |B_2\rangle \ .
\end{aligned} \tag{5}
$$

In the free-electron case $G=0=S$, and the GS of the system belongs to IR A_2; the same is true for $t=0=G$, and for the limit $G\to\infty$, where the GS corresponds to a CW. The BW states also belong to IR's A_2 or B_2. It can be shown that, even in the general case, the GS belongs to the $\mathcal{H}_2 = A_2 \oplus B_2$ electronic subspace. On that subspace the Hamiltonian is

$$
H[A_2 \oplus B_2] = \begin{bmatrix} -2t & -\sqrt{6}Su & \sqrt{2}Su & -2Su \\ -\sqrt{6}Su & -G & 0 & -\sqrt{6}t \\ \sqrt{2}Su & 0 & G & -\sqrt{2}t \\ -2Su & -\sqrt{6}t & -\sqrt{2}t & -2t \end{bmatrix} + \omega b^\dagger b \ , \tag{6}
$$

where the order $|B_2\rangle, |A_2,1\rangle, |A_2,2\rangle, |A_2,3\rangle$ is used for the basis vectors; we have omitted the additive constant $G+\omega/2$.

Using Eq. (6) and some algebra, the eigenenergy equation for Ψ_E can be cast as a tridiagonal equation for the coefficients β_n. It can be seen that $\beta_n/\beta_{n-2} \approx 2S^2/(n\omega^2)$ if $n \gg 4(S/\omega)^2$. Using this result, the tridiagonal matrix can be suitably truncated, thus obtaining the eigenfunctions of $H[A_2 \oplus B_2]$ with negligible error.

III. THE ADIABATIC APPROXIMATION

Let us analyze the properties of the model in the adiabatic limit of low phonon frequencies. For that purpose we write the phononic part of the Hamiltonian as $\omega(b^\dagger b + \frac{1}{2}) = Nu^2/2D + P^2/2M$, where $P = i\sqrt{N}(b^\dagger - b)/(2S) = -i\partial/\partial u$ is the momentum operator, $D = 2S^2/\omega$, and $M = N/(2\omega S^2)$. We initially disregard the kinetic energy of ions, $H \to H_0(u) = H - P^2/2M$. According to the BO approximation, the eigenvalues of $H_0(u)$, say $W_\alpha(u) \equiv E_\alpha(u) + Nu^2/(2D)$, correspond to the adiabatic potentials for the lattice. We are interested in the subspace of the GS, $\mathcal{H}_2$, and thus $E_\alpha(u)$ are the eigenvalues of matrix (6).

The shape of the adiabatic potential $W_\alpha(u)[=W_\alpha(-u)]$ provides a qualitative understanding of the lattice state. In particular, if the minimum of $W_\alpha(u)$ lies at $u=0$, then the lattice is undistorted; conversely, if $W_\alpha(u)$ ha two symmetric absolute minima for $u = \pm u_M \neq 0$, then the lattice is distorted, u_M being the amplitude of Peierls distortion.

We have verified numerically that the term $\partial^2 E_0/\partial u^2$ (which depends only on G) is always negative; it has a unique minimum at $u=0$, increasing monotonically as $|u|$ increases, and vanishing for $|u| \to \infty$. Therefore, $E_0(u)$ as a single maximum at $u=0$, and decreases linearly for $u \to \infty$. Using $(\partial^2 W_0/\partial u^2) = N/D + \partial^2 E_0/\partial u^2$, this behavior of $E_0(u)$ implies the following.

(i) If $D < -N/[\partial^2 E_0/\partial u^2]_{\{u=0\}} \equiv D_c(G)$, then $W_0(u)$ has positive curvature and no inflection points. Therefore, the GS adiabatic potential has only one minimum at $u=0$.

(ii) If $D > D_c(G)$, then $W_0(u)$ has exactly two (symmetric) inflection points, and negative curvature between them. Therefore, $W_0(u)$ has a maximum at $u=0$, and two minima at $u = \pm u_M$.

A. The adiabatic phase diagram

Figure 1 shows the adiabatic ($\omega=0$) phase diagram in the plane (D,G). The lower part is the undistorted region, separated from the BW phase by the curve $D_c(G)$. The upper region is the unphysical regime of large lattice deformations; its boundary is given by $t_{2l-1,2l}=0$, say $u_M = t$. We remark on four aspects related to Fig. 1.

(i) In the limit $G\to\infty$ the boundary between distorted and undistorted regimes adopts the asymptotic form $D_c(G) \sim \frac{1}{2}G$, in agreement with the exact result for the $N\to\infty$ limit.[9]

(ii) Spurious finite-size effects are present. In fact, for $G < 2t$ and $N\to\infty$, and infinitesimal e-ph interaction is enough to yield a BW.[9] In contrast, our six-site ring is undistorted for $D < 0.9t$. This effect is due to finite—instead of infinitesimal—separation between occupied and empty electronic levels.[7]

(iii) An amplification of the $G < 2t$ region (see the small rectangle inside Fig. 1) shows a minimum in the critical boundary $D_c(G)$ at $G \sim t$. Thus the BW state is especially enhanced at this intermediate value of G.

(iv) The existence of one or two minima in $W_0(u)$ implies that the transition between BW and undistorted phases is *continuous* (second order) in the present model (SSH e-ph coupling). In contrast, in the molecular crystal model (MCM), where intramolecular e-ph and e-e interaction are postulated, the existence of three minima in $W_0(u)$ is possible,[15,16] and therefore the transition to the distorted CW phase may be *discontinuous*. The latter result agrees with the analysis of a four-site ring.[23]

This difference between the MCM and SSH models can

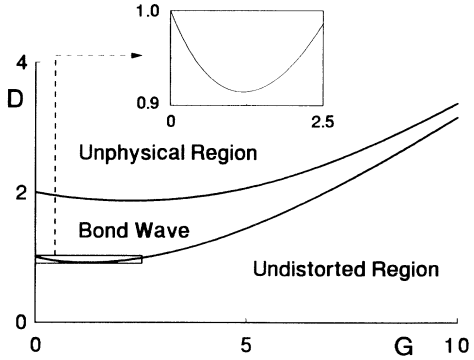

FIG. 1. The phase diagram in the $\omega \to 0$ limit. The lower and intermediate regions respect the undistorted and BW regimes, respectively. The upper region corresponds to unphysical large lattice deformations.

be understood as follows: The e-ph coupling of MCM leads to an *intramolecular attraction* between electrons.[1] Thus a large intramolecular e-ph coupling leads to double occupied or empty sites, while a large U leads to single occupation. Both kinds of states are orthogonal to each other and, for large e-e and/or e-ph couplings, a continuous transition between these states is ruled out.[24] This assertion is supported by the Hartree-Fock analysis of the $N=\infty$ extended Hubbard-MCM model.[25]

In contrast with the "direct competition"[13] between the e-e and e-ph interactions of MCM, the two extreme states of the SSH model (CW and BW) have some degree of compatibility, as confirmed by literature.[3,9,10] Also, from Eq. (5), it holds that $\langle \mathrm{BW},+|\mathrm{CW},+\rangle=\sqrt{\frac{2}{5}}$, and so an important mixing between BW's and CW's is present, allowing a *continuous* passage between them.

In Fig. 2 we show the four adiabatic potentials associated with the GS subspace $A_2\oplus B_2$. We choose $G=D=2$; therefore the GS corresponds to a BW. While the adiabatic potential of the GS has two symmetric minima, the other potentials, associated with electronic excitations, have only one minimum.

B. The Born-Oppenheimer analysis

We restore the lattice kinetic energy and add it to the adiabatic potential, thus obtaining the BO eigenenergy equation; see Eq. (A6) of the Appendix. This procedure allows one to recover (to some extent) typical quantum-mechanical effects, such as tunneling and zero-point energy. In addition, the BO GS provides a lower bound for the GS energy of the exact Hamiltonian.[26]

If $W_0(u)$ has two minima separated by a comparatively high central barrier, say $W_M \gg \omega$, then the lower eigenenergies of Eq. (A6) are grouped in narrow doublets. Let us denote these energies and eigenfunctions as

$$E^{\pm}_{0,n}=E_{0,n}\mp\Delta_n/2 \quad \text{and} \quad \xi^{\pm}_{0,n}=[\xi_{n,R}\pm\xi_{n,L}]/\sqrt{2}\ ,$$

respectively; here the energy split satisfies $\Delta_n \ll \omega$. These doublets persist as long as $E_{0,n}<W_0(0)$. The lattice function $\xi_{n,R}(u)$ is vanisingly small, except in a narrow neighborhood of the right minimum u_M, while $\xi_{n,L}(u)=\xi_{n,R}(-u)$ is strongly located on the left minimum. According to this behavior and Eq. (A2) of the Appendix, the wave function of the full system (e and ph parts) can be approximated by

$$|\Psi^{\pm}_{0,n}\rangle=[|f_0(u_M)\rangle|\xi_{n,R}\rangle\pm|f_0(-u_M)\rangle|\xi_{n,L}\rangle]/\sqrt{2}\ . \tag{7}$$

The state $\Psi^{+}_{0,n}$ belongs to the IR A_2, while $\Psi^{-}_{0,n}$ lies in B_2. In the limit of a fully dimerized lattice, $t=u_M$, it holds that $|f_0(u_M)\rangle=|\mathrm{BW},2\rangle$ and $|f_0(-u_m)\rangle=|\mathrm{BW},1\rangle$.

In general, the "tunneling time" for going from one minimum to the other is $\mathcal{T}_n\equiv\pi/\Delta_n\equiv\pi/[E_{0,n}(B_2)-E_{0,n}(A_2)]$. In the present case ($\omega\ll W_M$), the wave functions $\xi^{\pm}_{0,n}(u)$ are vanishingly small inside the central barrier; therefore, the states $\xi_{n,R},\xi_{n,L}$ are nearly stationary, and the tunneling time is much larger than the lattice vibration time, $\mathcal{T}_n\gg\pi/\omega$.

According to Eq. (7), the low-lying excited energy levels are basically vibrational in character. The separation between them can be roughly associated with some "effective" phonon frequency $\bar{\omega}_n=E_{0,n+1}-E_{0,n}$, which is smaller than the "bare" one ω. The effective vibrational time becomes $\pi/\bar{\omega}_n$. In the case of a BW, $\bar{\omega}_n$ is defined as the separation between adjacent doublets.

Figure 3 shows the 14 lowest quantum levels for the parameters of Fig. 2, $D=G=2$, and low frequency ($\omega=0.25$). The barrier height is $W_M=0.53$, and it traps the six lowest levels, which pair in three doublets. The GS doublet is very narrow, $\pi/\mathcal{T}=0.000\,16$. The "effective" frequency associated with the GS shows a 20% softening with respect to the "bare" one. In the case of Fig. 3, the exact quantum-mechanical (QM) and BO calculations coincide to a considerable extent; the results agree with Brattsev's theorem.[26]

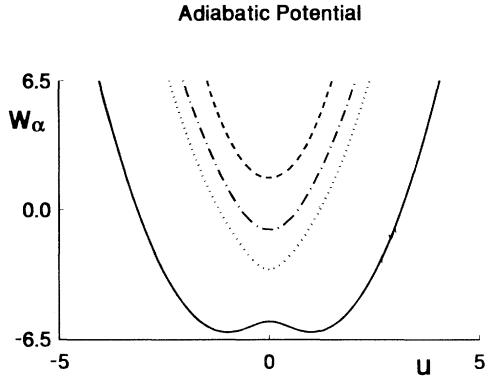

FIG. 2. The four adiabatic potentials associated with the invariant subspace $A_2\oplus B_2$. The system parameters are $G=D=2$.

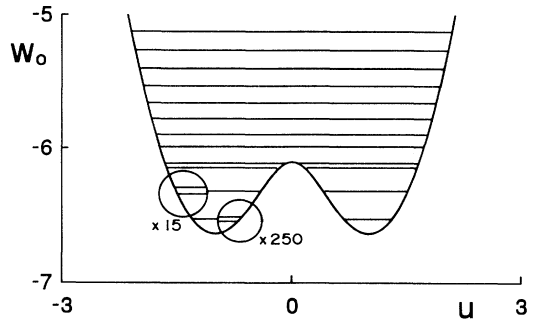

FIG. 3. The first 14 quantum levels for the lower adiabatic potential of Fig. 2, $D=G=2$. The frequency is $\omega=0.25$. An amplification is applied to the two lower doublets, in order to resolve them in individual levels.

IV. NONADIABATIC RESULTS

In this section we study the QM solution of the model. In particular, we characterize the GS properties by means of various averages. In addition, a comparison between exact and BO results is given. Roughly speaking,

the adiabatic description is qualitatively valid, and so it shall often be used to motivate the discussion.

A. The effect of phononic frequency

The adiabatic potentials $W_\alpha(u)$ are fully determined by fixing D and G, and their shape does not depend on the frequency ω or the ionic mass $M=N/(D\omega^2)$. As the frequency increases (e.g., if the ionic mass decreases), the separation between the energy levels also increases. In particular, in the BW region, and for a sufficient high frequency, the central barrier of $W_0(u)$ is surpassed by the GS level; in that case the system is no longer trapped in a minimum of the adiabatic potential, and the exchange time between the $|\mathrm{BW},1\rangle$ and $|\mathrm{BW},2\rangle$ states becomes comparable with the lattice oscillation time.

This qualitative description is well illustrated in Fig. 4(a), which shows a plot of $E_0(B_2)-E_0(A_2)\equiv\Delta_0\equiv\pi/\mathcal{T}$ versus frequency. The same parameters of Fig. 2 are chosen, $G=D=2$. The exact QM (dotted line) and BO (continuous line) calculations are compared. In order to amplify the low frequency behavior, a plot of $-\omega\ln(\Delta_0)$ is also included.

For low frequencies, the tunneling time is roughly governed by $\pi/\mathcal{T}=\Delta_0\sim W_M\exp[-cW_M/\omega]$, where the constant $c\sim 4$ in the case of Fig. 4(a). The doublet width remains very narrow, even for moderately high frequencies ω. For example, at $\omega\approx 0.4W_M$, the tunneling time corresponds to some 10 000 lattice vibrations; decreasing to seven lattice vibrations for frequencies as large as twice the barrier height. Indeed, for large enough ω both times nearly coincide, and the distinction between the BW and the undistorted lattice becomes ambiguous.

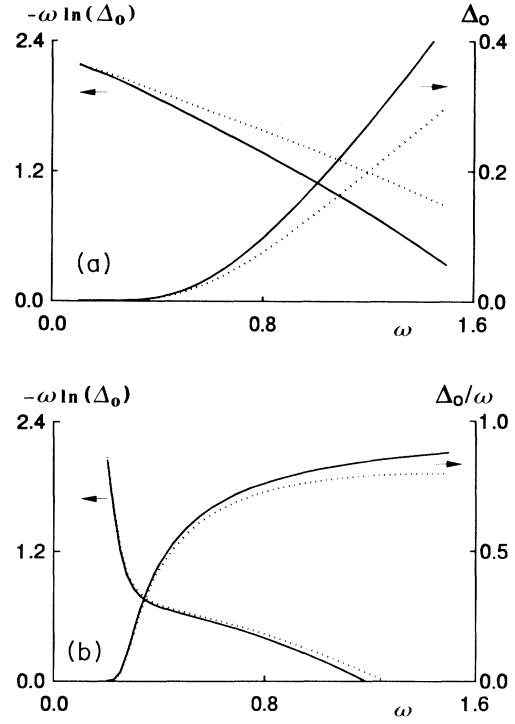

FIG. 4. The separation of the lower doublet $E_0(B_2)-E_0(A_2)\equiv\Delta_0$ vs ω. A plot of $-\omega\ln(\Delta_0)$ is also included. The QM and BO results appear as dotted and continuous lines, respectively. We fix the parameters $D=G=2$ in (a), and $S=0.44$, $G=0$ in Fig. (b). In order to test the asymptotic limit $\Delta_0\to\omega$ for $\omega\to\infty$, (b) shows the ratio Δ_0/ω.

The comparison between exact and BO results shows that the latter approximation works quite well in the low-frequency region (for example, $\Delta_{\mathrm{BO}}-\Delta_{\mathrm{QM}}=0.000\,06\omega=0.1\Delta_{\mathrm{BO}}$ at $\omega=0.25$). The error slowly increases with ω, so that $\Delta_{\mathrm{BO}}-\Delta_{\mathrm{QM}}=0.18=0.25\Delta_{\mathrm{BO}}$ for frequencies as high as $\omega=1$.

A major conclusion of Fig. 4 (supported by many other numerical calculations) is the fact that the BO prediction for the tunneling time *is always less than the exact QM calculations.* This is a surprising result, as one might expect that exact QM calculations should emphasize the tunneling effect in comparison to the somewhat "semiclassical" treatment of BO. However, this peculiar behavior is consistent with the analysis of the Appendix, where the QM problem appears as the solution of the BO Schrödinger equation under the proviso that the kinetic energy is modified by a "gauge field" $P^2/2M\to[\underline{I}P+\underline{A}(u)]^2/2M\equiv P^2/2M+\underline{V}_{\mathrm{NA}}$, with $P=(-i)\partial/\partial u$. Thus the nonadiabatic (NA) corrections to the BO approximation are embodied in $\underline{V}_{\mathrm{NA}}$. The diagonal part of this operator is responsible for the zeroth-order correction due to the nonadiabatic effects; it depends only on u, $\{\underline{V}_{\mathrm{NA}}\}_{\alpha,\alpha}=\langle\partial f_\alpha/\partial u|\partial f_\alpha/\partial u\rangle/2M\equiv V_{\alpha,\alpha}(u)$. However, instead of doing perturbation theory over $V_{\alpha,\alpha}$, we have included this operator exactly by adding it to the Born-Oppenheimer Hamiltonian $\underline{H}_{\mathrm{BO}}$, thus obtaining a "modified" adiabatic potential $W_\alpha(u)\to W_\alpha(u)+V_{\alpha,\alpha}(u)\equiv\overline{W}_\alpha(u)$.

This "modified adiabatic potential" can also be obtained by using the trial function $|\Psi_\alpha\rangle=\int du\,|u\rangle|f_\alpha(u)\rangle\xi_\alpha(u)$, and minimizing the energy average with respect to $\xi_\alpha(u)$. Therefore, the GS energy associated with the potential $\overline{W}_\alpha(u)$ is an upper bound for the exact (QM) energy of the GS, $\overline{E}_{0,0}>E_{0,0}(\mathrm{QM})>E_{0,0}(\mathrm{BO})$ (the last inequality is the Brattsev theorem).

Our numerical calculations for the low-energy levels confirm that the diagonal part of the nonadiabatic perturbation, $V_{0,0}(u)$ has a dominant role in accounting for the BO errors. In fact, replacing $W_0(u)\to\overline{W}_0(u)$ and using $D=G=2,\omega=0.5$, the GS energy error decreases 40 times and the tunneling time error decreases four times; while, for the highly nonadiabatic case $D=G=2,\omega=1.4$, the GS error decreases by a factor 10.

In particular, the fact that the BO calculation for the GS gives a *shorter tunneling time* than the QM result, $\mathcal{T}_{\mathrm{BO}}<\mathcal{T}_{\mathrm{QM}}$, can be qualitatively understood in terms of the nonadiabatic correction to the BO potential, $V_{0,0}(u)$, which is always positive and has a maximum at $u=0$. This implies that the "corrected" adiabatic potential $\overline{W}_0(u)$ has a more impenetrable barrier in comparison to that of $W_0(u)$. Thus the tunneling time for the "corrected" potential is longer than the BO result. We also note that the inequality $V_{0,0}(u)>0$ gives a qualitative explana-

tion of the Brattsev theorem.

Beyond numerical results, it is easy to convince oneself that the off-diagonal corrections coming from $\underline{V}_{NA}$ are small for the low-energy BW states; the latter one under the proviso $W_\alpha(0)-W_0(u_M)\gg\omega\ \forall\alpha$. Also, by using qualitative arguments, it can be seen that off-diagonal corrections produce a "compression" in the adiabatic doublet $E_{0,0}-E_{0,1}$, thus making an additional contribution that increases $\mathcal{T}_{QM}$ in comparison to $\mathcal{T}_{BO}$.

Figure 4(b) shows the width of the lower doublet Δ_0 versus ω for a fixed e-ph coupling, $S=0.44$, and $G=0$. This figure represents a collection of otherwise equivalent systems, but with different ionic masses. The dotted and continuous curves correspond to QM and BO calculations, respectively. Δ_0 shows a steeper rise with ω in Fig. 4(b) in comparison to Fig. 4(a), as is apparent by comparing the logarithmic curves. This behavior is due to the *decrease* of $D=2S^2/\omega$ as ω increases (S is now fixed); thus the central barrier of the adiabatic potential W_M also decreases with ω, disappearing at $\omega\approx 0.4$. For that value of ω, the curves show an inflection point.

B. The effect of Coulomb repulsion G

Figure 5 shows the separation between the GS, $E_0=E_0(A_2)$, and the three succeeding levels $[E_1=E_0(B_2)$, $E_2=E_1(A_2)$, and $E_3=E_1(B_2)]$ in terms of G for $D=2$ and $\omega=0.5$. The BO and QM results are represented by continuous lines and small circles, respectively. In the adiabatic limit, these parameters correspond to a BW for $0\le G\le 7$, while for $G>7$ the system is undistorted. Obviously the effect of a moderate or high frequency is to reduce the BW region, but then the BW boundary becomes blurred. In order to evaluate the degree of dimerization, we consider the ratio between tunneling and vibration times, which can roughly be defined as $R\equiv(E_2-E_1)/(E_1-E_0)=\bar{\omega}_1/\Delta_0\equiv\mathcal{T}/\mathcal{T}_V$, where $\bar{\omega}$ and $\mathcal{T}_V$ can be associated with the "effective" vibrational frequency and time, respectively. In the case of Fig. 5, $R(G=0)\approx 30$. A first increase in G leads to a slight maximum, $R(G=t)\approx 33$; from there on R decreases as G increases. This behavior confirms (for our nonadiabatic calculations) that a small or moderate G enhances the BW, while a larger G inhibits the BW.

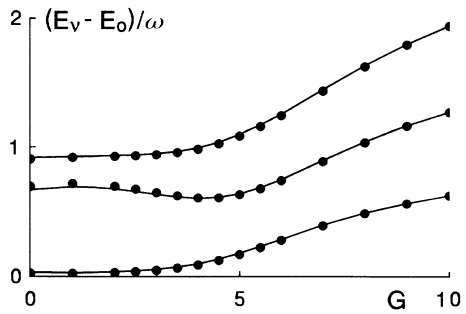

FIG. 5. The separation between the GS and the three succeeding levels, E_n-E_0; $n=1,2,3$ vs G for $D=2$ and $\omega=0.5$. The QM calculations appear as small circles, while the BO results are plotted in a full line.

At $G=4.5$ the second level surpasses the central barrier of $W_0(u)$, although the tunneling time is still appreciable, $R=4$. At $G=5.5$ the GS exceeds the adiabatic barrier, but some traces of a BW distortion persist, as then $R\approx 2$. This value of G is not too far from the adiabatic ($\omega=0$) boundary of the BW region, in spite of the relatively large value of ω considered here. The persistence of the BW for moderate frequencies is partially due to the "nonadiabatic" correction of the BO potential, which reinforces the central barrier responsible for dimerization.

The inequality $\mathcal{T}_{QM}>\mathcal{T}_{BO}$ is confirmed by Fig. 5, where the BO overestimates tunneling time by 25% for $G=0$. The BO error decreases as G increases; this is due to the fact that the e-ph interaction becomes ineffective as the Coulomb repulsion G increases, as then a CW appears, thus freezing electronic positions.

C. Nonadiabatic interaction among BO levels

In order to analyze the BO deviations at high frequencies, in Fig. 6 we compare the BO and QM results for the first 11 energy levels belonging to the IR's A_2 (left) and B_2 (right). We do that for $\omega=1.4$ and $D=G=2$. Each BO level can be associated rigorously with an adiabatic potential; in the case at hand, these potentials correspond to Fig. 2. Accordingly, we represent each BO level by means of the same type of line (continuous, dotted, broken dotted, or broken) used there. In spite of the high frequency (ω is 2.5 times larger than the adiabatic barrier W_M), it holds that $R=3.4$; therefore the system still shows a vestige of the BW. In addition, there is an appreciable softening (36%) in the phonon frequency.

According to Fig. 6, the QM and adiabatic energy levels coincide to an appreciable extent below the minimum of the second adiabatic potential. However, for higher energies the agreement declines, especially when two energy levels of the same symmetry, but associated with different adiabatic potentials, lie near each other. Such "accidential" coincidence is strongly removed by the perturbation operator $\underline{V}_{NA}$ of Eq. (A5), which generates a "repulsion" between adjacent levels of the same symmetry. The existence of other nearby levels may, however,

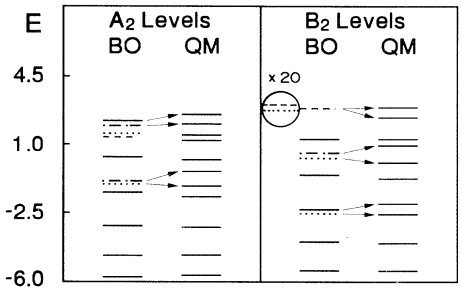

FIG. 6. The first 11 energy levels associated with the IR's A_2 (left) and B_2 (right) for the parameters $D=G=2$ and $\omega=1.4$. For each IR, both BO and QM results are shown. Each BO level is ascribed to one adiabatic potential of Fig. 2 by using the same type of line employed there (continuous, dotted, broken dotted, or broken).

compensate for this effect if they "push" in the opposite direction. In this highly nonadiabatic regime, the diagonal correction $W_0(u) \rightarrow \overline{W}_0(u)$ only improves the GS energy.

D. Order parameters for BW and CW states

Let us consider the following averages:

$$Q_1 = \frac{1}{N} \sum_l \langle c_l^\dagger c_l \; c_{l+1}^\dagger c_{l+1} \rangle \; ,$$
$$\tau_1 = \frac{2}{N} \sum_l \langle (c_l^\dagger c_{l+1} + \text{H.c.}) \rangle \; , \tag{8}$$
$$\tau_2 = \frac{1}{8N} \sum_l \langle [(c_{l-1}^\dagger c_l + c_l^\dagger c_{l-1})(c_l^\dagger c_{l+1} + c_{l+1}^\dagger c_l) + \text{H.c.}] \rangle \; .$$

Here Q_1 is the charge correlation and τ_2 is the charge-transfer correlation between neighboring bonds;[9] finally, τ_1 is a measure of electronic delocalization. These averages are evaluated with the GS. We now introduce the electronic order parameters Δ_{BW} and Γ_{CW}:

$$\Delta_{\text{BW}} = 4\sqrt{\tau_1^2 - 2\tau_2} \; ,$$
$$\Gamma_{\text{CW}} = \sqrt{1 - 4(Q_1 + \tau_1^2 + \Delta_{\text{BW}}^2)} \; , \tag{9}$$

which measure the strengths of BW's and CW's existing in the system. These relations, though applicable to the exact solution, are motivated by the Hartree-Fock definition of BW and CW order parameters:[10]

$$\langle c_l^\dagger c_{l+1} \rangle = \tau_1 + \tfrac{1}{4}(-1)^l \Delta_{\text{BW}}$$

and

$$\langle c_l^\dagger c_l \; c_{l+1}^\dagger c_{l+1} \rangle = \tfrac{1}{2}[1 + (-1)^l \Gamma_{\text{CW}}] \; .$$

In the limiting case of a net CW or BW, the corresponding order parameter attains its maximum value, $\Gamma_{\text{CW}} = 1$ or $\Delta_{\text{BW}} = 1$, respectively; in addition, $\tau_1 = \frac{1}{4}$ in the last case.

Figure 7 shows the dependence on G of both order parameters. We choose $D = 1.08$ and $\omega = 0.04$; thus the system lies slightly inside the BW region when $0 < G < 3.2$, being in the CW region for a larger G. Accordingly, the value of Δ_{BW} increases as the system goes into the BW region, decreasing when it emerges from that region. The maximum of Δ_{BW} is attained for $G \approx 2t$, thus confirming the assertion[9] that a first increase in G enhances the BW, while a further increase inhibits it.

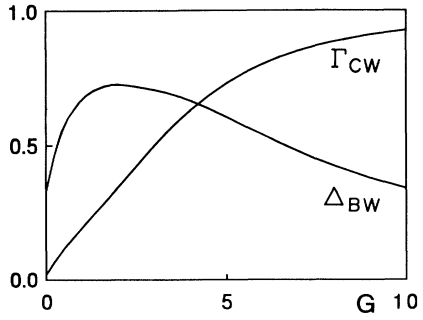

FIG. 7. The electronic order parameters Δ_{BW} and Γ_{CW} vs the Coulomb repulsion G for $D = 1.08$ and $\omega = 0.04$.

On the other hand, Γ_{CW} increases monotonically with G; this is quite natural, as a CW is enhanced by large values of G. Another remarkable feature of Fig. 7 is the coexistence of BW's and CW's in a broad (although blurred) region; this result agrees with the literature.[9,10]

E. Mean oscillation amplitudes

Another measure of lattice deformation is given by the ratio[16]

$$\mathcal{H} = \frac{\langle \check{X}^4 \rangle}{\langle \check{X}^2 \rangle^2}, \text{ where } \check{X} = b + b^\dagger \; , \tag{10}$$

where averages are taken over the GS. In contrast to the electronic parameters Γ_{CW} and Δ_{BW}, this magnitude is a *direct measure* of lattice deformations. In fact, let us return to Eq. (7); in the case of a small ω, the phononic functions $\xi_{0,R}$ and $\xi_{0,L}$ can be obtained by means of two unitary operators over the "bare" phonon vacuum $|0\rangle$,

$$|\xi_{0,R}\rangle = \exp[u_M(b^\dagger - b)\sqrt{N}/2S] \times \exp[\alpha\{(b^\dagger)^2 - b^2\}]|0\rangle \equiv \check{O}_2 \check{O}_1 |0\rangle \; , \tag{11}$$

where $\exp(\alpha) \equiv u_0$ is the new zero-point oscillation amplitude, and $\check{O}_1$ is the associated dilatation operator (connected with the change in the "effective" phonon frequency $\omega \rightarrow \overline{\omega}$). The operator $\check{O}_2$ shifts the positions in u_M. The "left" state $\xi_{0,L}$ is obtained by changing $u_M \rightarrow -u_M$ in Eq. (11).

It holds that $[\check{O}_2 \check{O}_1]^{-1} \check{X} \check{O}_2 \check{O}_1 = u_0 \check{X} \pm u_M$, where the signs + and − correspond to the states $\xi_{0,R}$ and $\xi_{0,L}$, respectively. Combining this relation with Eqs. (7) and (11), and assuming a negligible overlap between the states $\xi_{0,L}$ and $\xi_{0,R}$, it follows that $\langle \check{X}^2 \rangle = u_M^2 + u_0^2$ and $\langle \check{X}^4 \rangle = u_M^4 + 6u_M^2 u_0^2 + 3u_0^4$.

Introducing these expressions in Eq. (10), we conclude the following. (i) If the lattice is essentially undistorted, then $u_M \ll u_0$ and $\mathcal{H} \sim 3$. (ii) In the case of a strongly dimerized lattice, $u_M \gg u_0$ and $\mathcal{H} \sim 1$. Indeed, the preceding discussion becomes meaningless in the intermediate regime between undistorted and BW states, as large anharmonic effects then appear.

Figure 8(a) shows $\mathcal{H}$ versus G for $D = 1.08$, and $\omega = 0.04$ (the same parameters of Fig. 7). Accordingly, the behavior of $\mathcal{H}(G)$ is consistent with Fig. 7, as a BW is apparent for $0 < G < 2.5$, where $\mathcal{H} < 2$. The maximum in Δ_{BW} corresponds to the minimum in $\mathcal{H}(G)$ at $G = 1.2$. A further increase in G leads to a fast convergence of $\mathcal{H}$ toward the undistorted limit $\mathcal{H} = 3$. Figure 8(a) also includes a plot of the ratio between the tunneling and the lattice vibration times, $R = \mathcal{T}/\mathcal{T}_V$. This plot shows a good correlation with $\mathcal{H}$, showing a sharp maximum just at the minimum of $\mathcal{H}$. At its maximum, $R \approx 26$, the BW is rather well established. For $G \rightarrow \infty$, $R \rightarrow 1$, in agreement with the spectrum of an harmonic oscillator. The

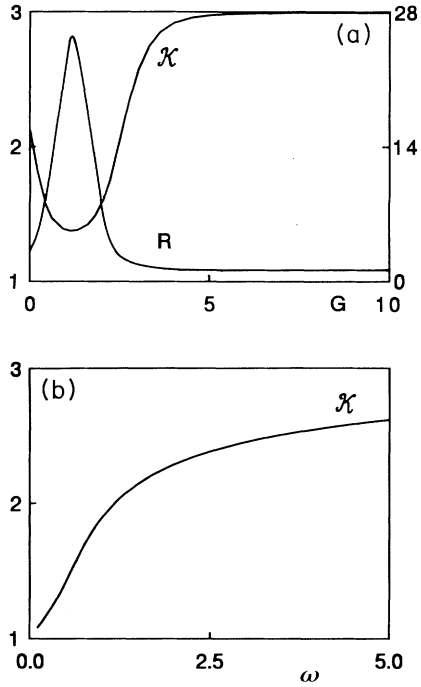

FIG. 8. (a) The parameters $\mathcal{K}$ (left axis) and R (right axis) vs G for $\omega=0.04$ and $D=1.08$. (b) The parameter $\mathcal{K}$ vs ω for $G=D=2$.

asymptotic limits of $\mathcal{K}$ and R are rapidly reached once the GS energy E_0 surmounts the central barrier of adiabatic potential.

Figure 8(b) represents $\mathcal{K}$ versus ω for $G=D=2$ [the same parameters of Fig. 4(a)]. In the low-frequency regime, the distorted limit ($\mathcal{K}=1$) is attained, as the system parameters lie in the BW region. When ω increases, $\mathcal{K}$ also increases, reaching the intermediate value $\mathcal{K}\sim 2$ when the second energy level E_1 surmounts the central barrier of the adiabatic potential. The undistorted limit $\mathcal{K}=3$ is slowly reached as $\omega\rightarrow\infty$.

V. SUMMARY AND CONCLUSIONS

The effect of nonadiabatic behavior in a Hubbard-Peierls system has been studied by means of a finite (six-site) ring. The exact QM solution of the eigenenergy problem was obtained, and contrasted with the BO approximation for the same cluster; therefore, QM and BO results are equally affected by finite-size effects, thus validating the comparison. Our main conclusions are the following.

(a) The image of a static Peierls BW is no longer applicable for a nonvanishing frequency $\omega\neq 0$, and the distinction between distorted and undistorted regimes becomes blurred to some extent. In particular, the bond waves $[1-2,3-4,5-6]$ and $[2-3,4-5,6-1]$ exchange in time. The tunneling time between these two distorted states, $\mathcal{T}$, was evaluated; it increases exponentially as $\omega\rightarrow 0$, $\ln(\mathcal{T})\propto 1/\omega$, being still large even for moderately high frequencies. However, in the thermodynamic limit $N\rightarrow\infty$, the quantum tunneling disappears at zero temperature; for $T\neq 0$; however, quantum tunneling contributes to the breaking of long-range order.[1]

(b) The appearance of a tiny central maximum in the adiabatic potential may be enough to stabilize a BW distortion. For example, a central barrier as small as $W_M=\frac{1}{2}\omega$ may yield a tunneling time as large as five lattice vibrations. Thus, despite the fact that the BW is somewhat inhibited in a spinless system,[11–13] our calculations show that relatively high frequencies are compatible with BW distortions.

(c) In contrast with the MCM, which present *first-order* phase transitions,[15,16] the present (SSH) model exhibits *second-order* phase transitions.

(d) For small or moderate frequencies, the BO and QM results agree to a considerable extent, especially if a "nonadiabatic" correction is introduced in the BO potential, $W_0(u)\rightarrow\overline{W}_0(u)$. This is especially true for low-energy states.

(e) The BO calculation overestimates the tunneling effect, *giving a shorter tunneling time than the exact QM results.* This is a surprising conclusion, as tunneling is a typical QM effect. We give an explanation of this result.

ACKNOWLEDGMENTS

This work has been supported by Fondecyt, Projects 90-1032 and 91-0832, and the DTI of the University of Chile, Project E-3053-9013.

APPENDIX: NONADIABATIC CORRECTIONS TO BORN-OPPENHEIMER APPROXIMATION

Let us analyze the general problem of electron-phonon interaction; for simplicity we consider only one lattice degree of freedom, $\check{Q}$, conjugated to the momentum $\check{p}$. We start from the general Hamiltonian

$$\check{H}=\check{H}_0(\{\text{electronic variables}\},\check{Q})+\frac{\check{p}^2}{2M}\ , \tag{A1}$$

where M is the ionic mass. For each eigenvalue q of the position operator $\check{Q}$, the eigenvectors of $\check{H}_0(q)$, say $\{|f_\alpha(q)\rangle\}$, constitute a complete basis of the electronic Hilbert space; here $\check{H}_0(q)|f_\alpha(q)\rangle=W_\alpha(q)|f_\alpha(q)\rangle$. Thus an eigenvector of the whole Hamiltonian (A1), $\check{H}|\Psi_E\rangle=E|\Psi_E\rangle$, can be written as

$$|\Psi_E\rangle=\int_{-\infty}^{\infty}dq\sum_\alpha|q\rangle|f_\alpha(q)\rangle\xi_{\alpha,E}(q)\ , \tag{A2}$$

where $\{|q\rangle\}$ is the position basis of lattice variables, $\check{Q}|q\rangle=q|q\rangle$. Using a procedure similar to that of Ref. 27, the eigenenergy equation for Ψ_E can be represented as

$$E\vec{\xi}_E(q)=\left\{\underline{W}(q)+\frac{1}{2M}\left[\underline{I}(-i)\frac{\partial}{\partial q}+\underline{A}(q)\right]^2\right\}\vec{\xi}_E(q)$$
$$\equiv\underline{H}\vec{\xi}_E\ , \tag{A3}$$

where $\vec{\xi}_E(q)$ is a column vector; $\{\vec{\xi}_E\}_\alpha=\xi_{\alpha,E}(q)$, $\{\underline{I}\}_{\alpha,\beta}=\delta_{\alpha,\beta}$ is the identity matrix, $\{\underline{W}\}_{\alpha,\beta}=\delta_{\alpha,\beta}W_\alpha(q)$, and the "gauge field" $\underline{A}$ is given by

$$\{\underline{A}\}_{\alpha,\beta}=-i\left\langle f_\alpha\left|\frac{\partial f_\beta}{\partial q}\right.\right\rangle$$

$$=\frac{i}{W_\alpha(q)-W_\beta(q)}\langle f_\alpha(q)|\frac{\partial \underline{H}_0}{\partial q}|f_\beta(q)\rangle \quad \text{(A4)}$$

for $\alpha\neq\beta$. We can choose $A_{\alpha,\alpha}=0$ by means of suitable phase factors in the basis vectors $|f_\alpha\rangle$. Equation (A3) is exact; we recast it as

$$\underline{H}=\underline{W}-\frac{1}{2M}\frac{\partial^2}{\partial q^2}+\underline{V}_{\rm NA}\equiv\underline{H}_{\rm BO}+\underline{V}_{\rm NA}\ . \quad \text{(A5)}$$

Here $\underline{V}_{\rm NA}=[\underline{A}^2+\check{p}\underline{A}+\underline{A}\check{p}]/2M$ is the *nonadiabatic perturbation.* Neglecting $\underline{V}_{\rm NA}$, we attain the BO approximation

$$\left[W_\alpha(q)-\frac{1}{2M}\frac{\partial^2}{\partial q^2}\right]\xi_{\alpha,n}(q)=E_{\alpha,n}\xi_{\alpha,n}(q)\ . \quad \text{(A6)}$$

The index α is now a quantum number for the electronic variables, and the associated electronic eigenvalue $W_\alpha(q)$ plays the role of a potential for lattice displacements. The index n numbers the "vibronic" energy levels associated with a fixed α.

The nonadiabatic perturbation $\underline{V}_{\rm NA}$ mixes the different "adiabatic solutions" $\xi_{\alpha,n}(q)$. This mixing is usually small for a large ionic mass M, as the function $\xi_{\alpha,E}(q)$ is then sharply peaked around the minimum of the adiabatic potential $W_\alpha(q)$, while the other magnitudes appearing in Eq. (A5), W_α, H_0, and $|f_\alpha\rangle$, have a smooth dependence on q.

[1]P. Lee, T. Rice, and P. W. Anderson, Phys. Rev. Lett. **31**, 462 (1973).

[2]W.-P. Su, J. R. Schrieffer, and A. J. Heeger, Phys. Rev. B **22**, 2099 (1980).

[3]S. Kivelson, Phys. Rev. B **28**, 2653 (1983).

[4]V. Waas, J. Voit, and H. Büttner, Synth. Met. **27**, A21 (1988), and references therein.

[5]S. Zhang, S. Kivelson, and A. Goldhaber, Phys. Rev. Lett. **58**, 2134 (1987).

[6]S. Dixit and S. Mazumdar, Phys. Rev. B **29**, 1824 (1984).

[7]Z. Soos and G. Hayden, Phys. Rev. B **40**, 3081 (1989).

[8]S. Mazumdar and D. Campbell, Phys. Rev. Lett. **55**, 2067 (1985).

[9]E. Gagliano, C. Proetto, and C. Balseiro, Phys. Rev. B **36**, 2257 (1987).

[10]J. Rössler and D. Gottlieb, J. Phys. Condens. Matter **2**, 3723 (1990).

[11]J. Hirsch and E. Fradklin, Phys. Rev. Lett. **49**, 402 (1982).

[12]E. Fradklin and J. Hirsch, Phys. Rev. B **27**, 1680 (1983); **27**, 4302 (1983).

[13]J. Hirsch, Phys. Rev. Lett. **51**, 296 (1983).

[14]J. Hirsch and M. Grabowski, Phys. Rev. Lett. **52**, 1713 (1984).

[15]W. Schmidt and M. Schrieber, Z. Phys. B **62**, 423 (1986).

[16]L. Falicov and C. Proetto, Phys. Rev. B **39**, 7545 (1989).

[17]J. Rice and E. Mele, Phys. Rev. B **25**, 1339 (1982).

[18]Peierls distortion can be frustrated by electronic transference beyond first neighbors; see D. Gottlieb and F. Melo, Nuovo Cimento **10D**, 1427 (1988).

[19]J. Hirsch and D. Scalapino, Phys. Rev. B **29**, 5554 (1984); **27**, 7169 (1983).

[20]G. König and G. Stollhoff, Phys. Rev. Lett. **65**, 1239 (1990).

[21]According to Ref. 10, the *e*-ph interaction reduces the lattice parameter, thus increasing t enough to prevent this unphysical situation.

[22]M. Tinkham, *Group Theory and Quantum Mechanics* (McGraw-Hill, New York, 1964).

[23]J.-I. Takimoto and Y. Toyozawa, J. Phys. Soc. Jpn. **52**, 4331 (1983).

[24]J. Hirsch, Phys. Rev. Lett. **53**, 2327 (1984).

[25]P. Venegas, J. Rössler, and C. Henríquez (unpublished).

[26]S. Epstein, J. Chem. Phys. **44**, 836 (1966).

[27]P. Lévay, Phys. Rev. A **45**, 1339 (1992).